

## Reducing the cytotoxicity of inhalable engineered nanoparticles via in situ passivation with biocompatible materials



Jeong Hoon Byeon <sup>a,\*</sup>, Jae Hong Park <sup>b</sup>, Thomas M. Peters <sup>b</sup>, Jeffrey T. Roberts <sup>c,\*\*</sup>

<sup>a</sup> School of Mechanical Engineering, Yeungnam University, Gyeongsan 712-749, Republic of Korea

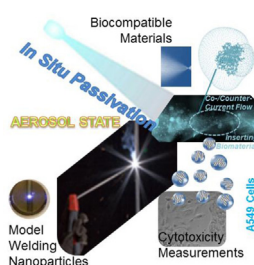
<sup>b</sup> Department of Occupational and Environmental Health, University of Iowa, IA 52242, United States

<sup>c</sup> Department of Chemistry, Purdue University, IN 47907, United States

### HIGHLIGHTS

- The cytotoxicity of model welding particles was modulated through in situ passivation.
- Model welding particles were incorporated with chitosan nanoparticles for passivation.
- In vitro assay revealed that the passivated particles had a lower cytotoxicity.
- Passivation with chitosan adhesive or graphite paste could also reduce cytotoxicity.
- This method would be suitable for efficient reduction of inhalable toxic components.

### GRAPHICAL ABSTRACT



### ARTICLE INFO

#### Article history:

Received 29 October 2014

Received in revised form 9 March 2015

Accepted 11 March 2015

Available online 12 March 2015

#### Keywords:

Reducing cytotoxicity

In situ passivation

Model welding nanoparticles

Chitosan

Average cell viability

### ABSTRACT

The cytotoxicity of model welding nanoparticles was modulated through in situ passivation with soluble biocompatible materials. A passivation process consisting of a spark discharge particle generator coupled to a collision atomizer as a co-flow or counter-flow configuration was used to incorporate the model nanoparticles with chitosan. The tested model welding nanoparticles are inhaled and that A549 cells are a human lung epithelial cell line. Measurements of in vitro cytotoxicity in A549 cells revealed that the passivated nanoparticles had a lower cytotoxicity (>65% in average cell viability, counter-flow) than the untreated model nanoparticles. Moreover, the co-flow incorporation between the nanoparticles and chitosan induced passivation of the nanoparticles, and the average cell viability increased by >80% compared to the model welding nanoparticles. As a more convenient way (additional chitosan generation and incorporation devices may not be required), other passivation strategies through a modification of the welding rod with chitosan adhesive and graphite paste did also enhance average cell viability (>58%). The approach outlined in this work is potentially generalizable as a new platform, using only biocompatible materials in situ, to treat nanoparticles before they are inhaled.

© 2015 Elsevier B.V. All rights reserved.

### 1. Introduction

Nanoparticles are ubiquitous in the environment, as they are emitted from several sources and also are formed by spontaneous nucleation in the atmosphere. There is increasing interest in

\* Corresponding author. Tel.: +82 53 8102451; fax: +82 53 8104627.

\*\* Corresponding author. Tel.: +1 765 4941730; fax: +1 765 4941736.

E-mail addresses: [postjb@yu.ac.kr](mailto:postjb@yu.ac.kr) (J.H. Byeon), [jtrob@purdue.edu](mailto:jtrob@purdue.edu) (J.T. Roberts).

measuring the impact of incidental and engineered nanoparticles on health [1,2]. Environmental and occupational exposures to metallic nanoparticles through inhalation have been associated with bronchitis, metal fume fever, occupational asthma, cancer and possible increases in lung tumorigenicity, suppression of lung defenses, and functional changes in the lung [3,4]. Engineered nanoparticles that are produced must be controlled and captured to minimize harmful effects to workers. Nanoparticles with metallic components including chromium (Cr), copper (Cu), iron (Fe), manganese (Mn), zinc (Zn), and nickel (Ni) can be found in ambient particulate matter, workplace air samples collected during the handling of engineered nanomaterials, or in fume from welding processes [5].

Welding is a common industrial process used to join metals. Over 300,000 workers in the US and millions of workers worldwide are exposed to welding particles on a daily basis [6]. Welding produces a large number of nanoparticles, which have a high probability of depositing in the sensitive alveolar region of the lung [7]. Welding particles are complex, composed of different metals, depending on the welding processes and materials used. Many metals present in welding fume particles are of interest toxicologically due to their potential adverse effects on worker health. The toxic effects of welding nanoparticles are due to their composition, which generates free radicals [8]. Several approaches have been used in an attempt to reduce the adverse health effects from inhaling welding fume [7]. Alterations in shielding gas composition is widely used to modify particle formation rate, although it does not significantly affect the fraction or composition of nanoparticles emitted by a welding process [9,10]. Ventilation systems can also be employed to reduce exposure; however, their effectiveness varies greatly because welders work in a vastly different locations and circumstances that cannot be easily controlled [11].

Different chemical and biological coatings on the surface of a nanoparticle can modify its toxicity since the surface clearly related to the toxic effects of the nanoparticles. Previous reports employed polymeric coatings on silver nanoparticles to reduce their cytotoxic effects on mammalian cells [12]. These interesting observations revealed the importance of the surface coating in determining nanoparticle induced toxicity. Most recently, silica ( $\text{SiO}_2$ ) coating on welding nanoparticles was introduced to decrease toxicity [7]. However, the strategy is not an on-site process, and moreover, molecular  $\text{SiO}_2$  precursors are toxic, and thus, it is still a challenge to develop an *in situ* passivation strategy from biocompatible/inert materials under effective and generalizable manners.

In this work, we describe an *in situ* approach to reduce the toxicity of model welding nanoparticles by merging them with biocompatible chitosan droplets. Chitosan was selected as a passivation material since chitosan, a natural, biocompatible, and biodegradable polymer, is widely used in biomedical applications as chitosan-based nanomaterials [13]. Furthermore, a previous study reported that chitosan nanoparticles are compatible with respiratory epithelial cells *in vitro*, and this encouraged choosing chitosan as a candidate for passivating model welding nanoparticles [14]. The model nanoparticles were produced using a spark discharge under air flow [15,16]. Spark discharge has been used to produce a variety of metallic, carbonaceous, and other materials with nanoscale dimensions at ambient temperatures and pressures. A previous report has shown that the simulated nanoparticles are good mimics for workplace-produced nanoparticles derived from commercial welding rods [16]. The particle-laden flow was directly mixed with chitosan droplets in co-flow and counter-flow configurations to passivate the surface of the nanoparticles. The physicochemical properties of size distribution, morphology, and composition, and the cytotoxic effects on the human lung carcinoma (A549) cell line of the passivated particles were evaluated. The cytotoxicity was further evaluated for nanoparticles from

modified welding rods with chitosan adhesive or graphite paste because it might induce a simpler and more practical procedure if the nanoparticles show a lower toxicity. This passivation technique may hold promise to reduce the toxicity of a wide range of engineered and incidental nanoparticles.

## 2. Experimental

### 2.1. Passivation of model welding nanoparticles

The rods, which were 6.35 mm in diameter and 100 mm in length, were obtained from Hobart, US. The air flow rate, which was controlled by a mass flow controller (Tylan, US), was  $3 \text{ L min}^{-1}$ . The specifications of the discharge configuration were as follows: resistance,  $0.5 \text{ M}\Omega$ ; capacitance,  $1.0 \text{ nF}$ ; loading current,  $3.0 \text{ mA}$ ; applied voltage,  $4.5 \text{ kV}$ ; and frequency,  $1320 \text{ Hz}$ .

In a spark channel, high temperature vapor is generated from the melting tip of a welding rod. This vapor cools rapidly during diffusion to the region surrounding the spark. Primary particles are then formed by nucleation from the vapor. The particle concentration depends on the mass fraction of the vapor ( $C$ ), is given as [17]

$$C = \frac{p_v M_v}{p_v M_v + (p_{\text{atm}} - p_v) M_g} \quad (1)$$

where  $p_v$  and  $p_{\text{atm}}$  are the partial pressure of the vapor [a function of the spark channel temperature ( $T_{\text{spark}}$ )] and atmospheric pressure, respectively, and  $M_v$  and  $M_g$  are the molecular weights of the vapor and the gas, respectively. The spark channel temperature can be estimated by the following formula:

$$T_{\text{spark}} = \left( \frac{E_d}{C_v v_{\text{spark}} \rho_g} \right) + T_0 \quad (2)$$

where,  $E_d$  is the discharge energy,  $C_v$  is the specific heat at constant volume,  $v_{\text{spark}}$  is the volume of the spark channel,  $\rho_g$  is the gas density, and  $T_0$  is the gas temperature.

To passivate the particles, the discharge-produced nanoparticle-laden air flow was mixed with chitosan droplets in a co-flow (mixing A) or counter-flow (mixing B) configuration (Fig. 1). In the co-flow configuration, the particle-laden flow ( $2 \text{ L min}^{-1}$ ) was used as the operating gas for collison atomizing a solution containing  $0.1 \text{ g}$  of chitosan (Mw: 15,000 Da, degree of deacetylation: 87%, Polysciences, US) dissolved in  $100 \text{ mL}$  of  $1 \text{ v/v\%}$  acetic acid solution. The degree of deacetylation is similar to that in a previous study (86%) [14], and this implies that the passivation warrants further investigation because the degree of deacetylation determines how the biopolymer can be applied [18]. The particles passed over the atomizer orifice, where they mixed with atomized droplets and  $2 \text{ L min}^{-1}$  of particle-free air to form hybrid droplets [19]. In the counter-flow configuration, the passivation was mainly processed via agglomeration between the model particles and chitosan droplets. To fabricate the model particles,  $2 \text{ L min}^{-1}$  of air injected into the spark chamber to carry the spark-produced particles while another  $2 \text{ L min}^{-1}$  of air passed over the atomizer orifice to produce chitosan droplets being formed hybrid droplets by merging the two flows. The hybrid droplets then passed through a mixing chamber to drive solvent from the droplets.

In order to verify feasibility of one of realistic strategies, commercial welding electrodes were modified to produce passivated welding particles (Fig. 2). Chitosan adhesive [20] (rod A) and graphite paste (51,010, LGB, Germany) (rod B) was used as passivation materials. Briefly, chitosan (Polysciences, US) was dissolved in  $1 \text{ w/v\%}$  in a water solution containing acetic acid ( $2 \text{ v/v\%}$ ) and indocyanine green ( $0.02 \text{ w/v\%}$ ). The gelatinous chitosan solution was stirred for  $6 \text{ h}$  before insertion. Chitosan adhesive and

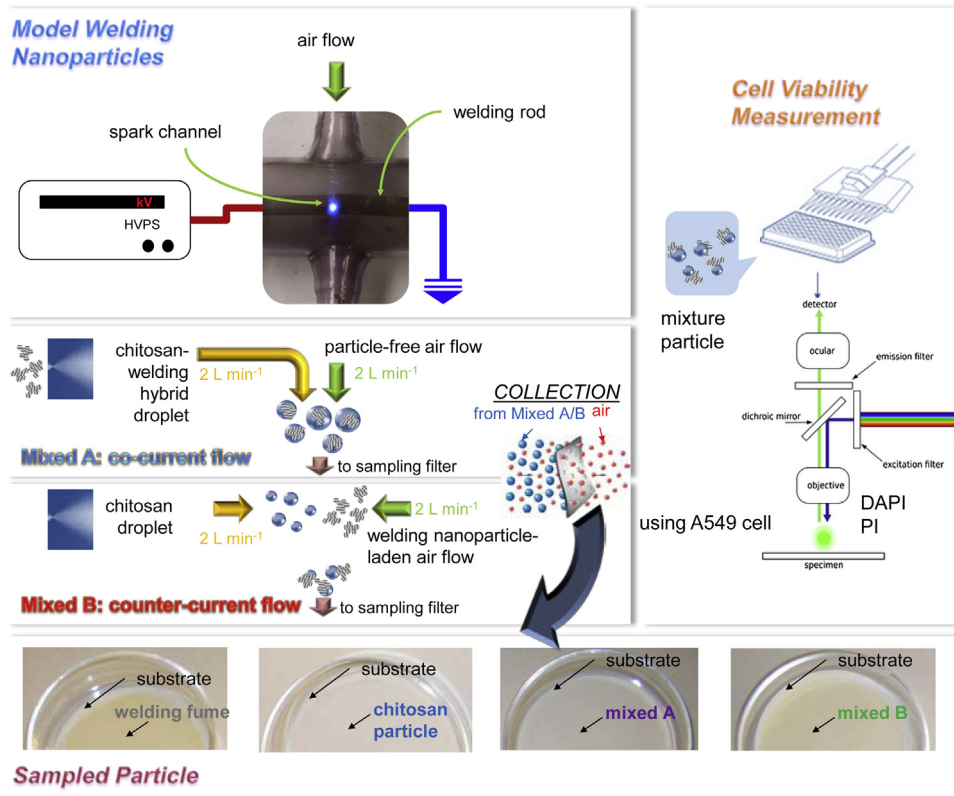


**Fig. 1.** Production, passivation, and toxicity assessment of model welding nanoparticles. The nanoparticles were produced using a spark discharge between commercial welding rods. The passivation using biocompatible materials was performed using a co-flow or counter-flow mixing of spark produced nanoparticles and collision atomized chitosan droplets. A549 cells were incubated with the sampled nanoparticles to measure average cell viability using a fluorescence microscopy.

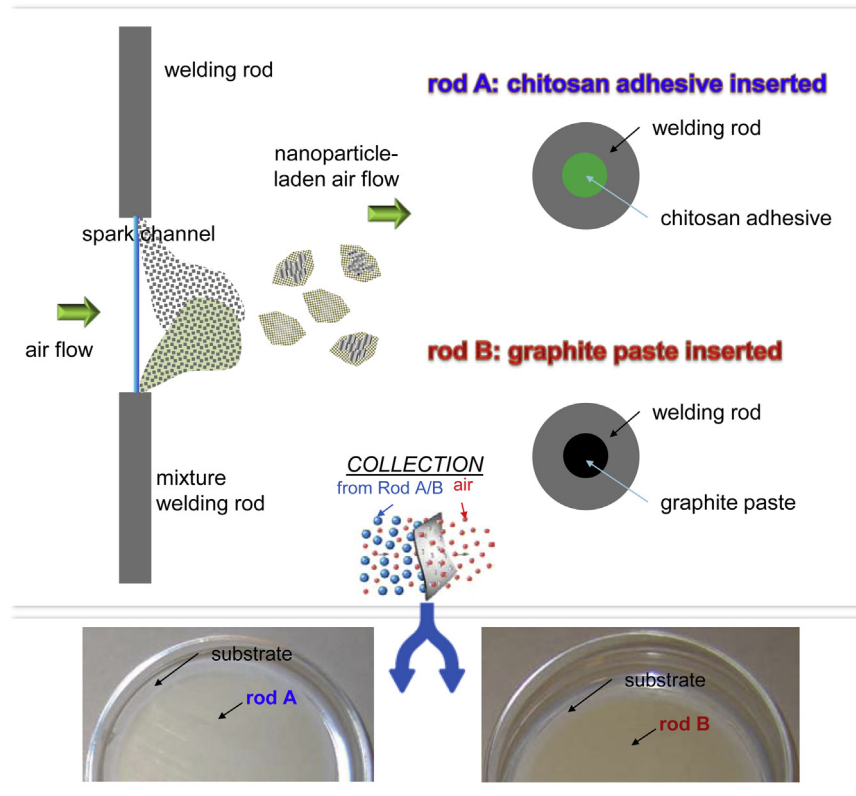


**Fig. 2.** Other passivations of model welding nanoparticles through the insertion of chitosan adhesive (rod A) or graphite paste (rod B) in a welding rod being used for spark discharge. A549 cells were incubated with the sampled nanoparticles to measure average cell viability.

purchased graphite paste were inserted into the hole (2 mm diameter and 10 mm length) drilled in the welding rod (as cathode). Those were then dried for 6 days under clean ambient conditions. The so-prepared cathode was spark sublimated afterwards.

For cytotoxicity measurements, samples were collected on a polytetrafluoroethylene (PTFE) membrane filter (0.2  $\mu\text{m}$  pore size, 47 mm diameter, 11,807-47-N, Sartorius, Germany) by physical filtration (i.e. mechanical filtration mainly by diffusion, of particles on the surfaces of the substrate).

## 2.2. Characterization of the model and passivated welding nanoparticles

The size distributions of the particles were measured using a scanning mobility particle sizer (SMPS), consisting of an electrostatic classifier (3081, TSI, US), a condensation particle counter (3022 A, TSI, US), and an aerosol charge neutralizer (4530, HCT, Korea). The SMPS system, which measures particle equivalent mobility diameter, was operated at a sample flow of 0.3  $\text{L min}^{-1}$ , a sheath flow of 3.0  $\text{L min}^{-1}$ , and a scan time of 135 s (measurement range: 15.1–661.2 nm). Transmission electron microscope (TEM, Libra 120, Carl Zeiss, Germany) images were obtained at an accelerating voltage of 120 kV. Specimens were prepared for examination in the TEM by direct electrostatic aerosol sampling at a sampling flow of 0.5  $\text{L min}^{-1}$  and an operating voltage of 5 kV using a Nano Particle Collector (NPC-10, HCT, Korea). For Fourier transform infrared spectroscopy (FTIR) analysis, IR spectra were recorded of powder samples on PTFE substrates (Figs. 1 and 2) under identical mass conditions. The mass of particles ( $m$ ) was measured using a microbalance (DV215CD, Ohaus, Switzerland) and also estimated via the following equation:

$$m = Q \times t_s \int_0^\infty \eta(D_p) C(D_p) dD_p \quad (3)$$

where  $Q$  is the flow rate of air,  $t_s$  is the sampling time,  $\eta(D_p)$  is the fractional collection efficiency, and  $C(D_p)$  is the number concentration of particles. Spectra were recorded on a IFS 66/S spectrometer (Bruker Optics, Germany). Spectra were obtained for samples in the range of 4000–400  $\text{cm}^{-1}$  in absorbance mode.

## 2.3. In vitro cell viability

Before in vitro cytotoxicity measurements, the sampled nanoparticles on a PTFE substrate were detached in an ultrasound bath for 10 s. Nanoparticles were dispersed in complete cell culture medium (CCM) RPMI 1640 with 2 mM L-glutamine (Life Technologies, US), with 5% fetal bovine serum (FBS, Sigma-Aldrich, US) and 1 v/v% 10,000 U  $\text{mL}^{-1}$  Penicillin and 10,000 U  $\text{mL}^{-1}$  Streptomycin (Life Technologies, US). All operations were performed in a class II biological safety cabinet (Nuaire, US). Welding rods and PTFE substrates were sterilized using UV-C (254 nm) radiation for 1 h before the experiments.

Cells were cultured in complete CCM composed of RPMI 1640 with L-glutamine supplemented with 10 v/v% FBS and 1 v/v% 10,000 U  $\text{mL}^{-1}$  Penicillin and 10,000 U  $\text{mL}^{-1}$  Streptomycin. Cells were maintained under standard cell culture conditions (5%  $\text{CO}_2$ , 95% humidity, and 37 °C) and passaged weekly. The cytotoxicity induced by nanoparticles was investigated by 3-(4,5-dimethylthiazol-2-yl)-2,5-diphenyltetrazolium bromide (MTT) assay. Cells ( $4.0 \times 10^4$  cells  $\text{mL}^{-1}$ ; 0.1 mL well $^{-1}$  in complete CCM) were seeded in 96-well plates. In the MTT assay, after 60 h incubation CCM was replaced with fresh medium contacting nanoparticles at concentrations of nanoparticles ranging from 5 to 200  $\mu\text{g mL}^{-1}$ . The range of concentrations was chosen for the cell viability assay based on a previous report [14].

regarding inhalation toxicity of aerosol chitosan particles. After 24, 48, and 72 h continuous exposure to nanoparticles, medium was removed, cells were washed with phosphate buffered saline (PBS) and then incubated with CCM containing 20% MTT solution (0.5 w/v% MTT  $\text{mL}^{-1}$  PBS; Sigma-Aldrich, US). After 3 h incubation, 0.1 mL lysis buffer [20 w/v% sodium dodecyl sulfate (SDS) dissolved in 50 mL deionized water and supplemented with 50 mL N,N-dimethylformamide] per well was added. Cells were further incubated overnight. A 10% dimethyl sulfoxide solution was used as positive control. Absorbances were measured at 570 nm with a reference wavelength at 690 nm by an ELISA plate reader (Thermo Multiskan Spectrum, US). In order to avoid misinterpreting the results cytotoxicity data were verified with at least three independent tests. Results were analyzed as the average of viability (% of the untreated control  $\pm$  standard deviation), and  $p$  values were also calculated. The Student's  $t$ -test was performed to determine statistical significance between untreated and treated groups.  $p < 0.05$  was regarded as statistically significant.

To further evaluate the effect of passivation on cell viability, two specific dyes, DAPI [4'-6-diamidino-2-phenylindole (Sigma-Aldrich, US)] and PI [propidium iodide (BD Science, US)], were employed to verify viability of cells with pure and chitosan-incorporated nanoparticles. DAPI (blue-350 nm) stains both live and dead cells, while PI (red-488 nm) may only pass through the membranes of dead cells and by examining the fluorescence, cell viability was also confirmed. Cells were suspended in DAPI ( $10^{-4}$  w/v%)/PI ( $5 \times 10^{-3}$  w/v%) solution, 0.1% Triton X-100 and incubated in the dark for 5 min. Stained cells were spotted onto a slide and allowed to dry. The stained welding particle-conjugated and non-conjugated cell suspensions with the two specific dyes were used to subsequently enumerate the dead cells (PI-positive cells) out of the total cells (DAPI-positive cells) bound to the welding particles via fluorescence microscopy (Carl Zeiss, Germany) analysis.

## 3. Results and discussion

Fig. 3 summarizes the size distributions of model welding nanoparticles before and after passivation with chitosan. The geometric mean diameter (GMD), geometric standard deviation (GSD), and total number concentration (TNC) of the welding nanoparticles were 43.9 nm, 1.54, and  $1.40 \times 10^7 \text{ cm}^{-3}$ , respectively (Table 1). The analogous data for individual chitosan particles were 97.9 nm, 1.66, and  $0.37 \times 10^7 \text{ cm}^{-3}$ , respectively, and for "mixed A particles (or mixed B particles)" they were 37.6 (45.4) nm, 1.82 (2.05), and 1.15 (1.17)  $\times 10^7 \text{ cm}^{-3}$ , respectively. The mixing of the particles generated a change in the size distribution. The "mixed B" particles showed a bimodal distribution (showing a larger GSD value than those in the other cases) which may have originated from individual welding (the smallest mode) and chitosan components (the larger mode). For "mixed B", in other words, although a large proportion of the chitosan droplets were incorporated with welding nanoparticles, some of the chitosan droplets remain in the initial

**Table 1**

A summary of the size distributions of spark produced model welding nanoparticles, collision atomized chitosan particles, and their mixing in a co-flow (mixing A) and counter-flow (mixing B) configuration.

Case	GMD <sup>a</sup> (nm)	GSD <sup>b</sup>	TNC <sup>c</sup> ( $\text{cm}^{-3}$ )
Model welding particle	$43.9 \pm 1.2$	$1.54 \pm 0.02$	$1.40 \times 10^7$
Chitosan particle	$97.9 \pm 2.6$	$1.66 \pm 0.02$	$0.37 \times 10^7$
mixed A	$37.6 \pm 0.9$	$1.82 \pm 0.01$	$1.15 \times 10^7$
mixed B	$45.4 \pm 1.4$	$2.05 \pm 0.01$	$1.17 \times 10^7$

\*Results are expressed as mean  $\pm$  SD from at least three independent experiments.

<sup>a</sup> Geometric mean diameter.

<sup>b</sup> Geometric standard deviation.

<sup>c</sup> Total number concentration.

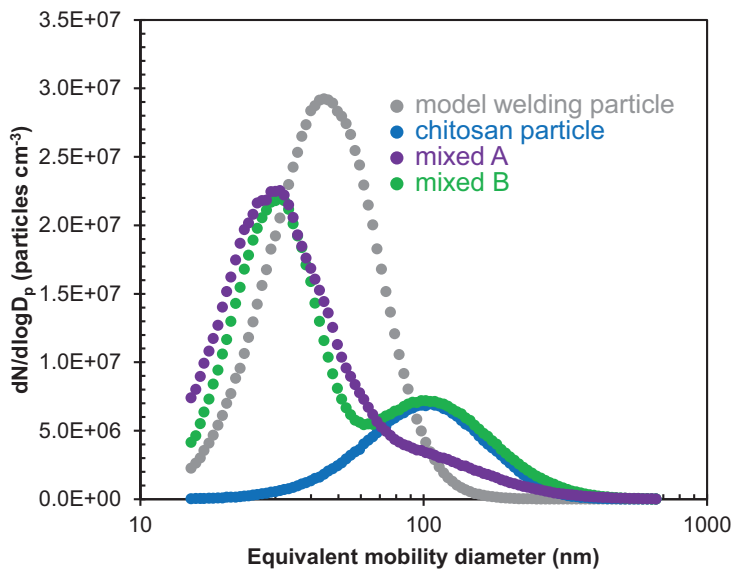


**Fig. 3.** Size distributions of spark produced model welding nanoparticles, collision atomized chitosan particles, and their mixing in a co-flow (mixing A) or counter-flow (mixing B) configuration.

state. This implies that the mixing configuration was not suitable to incorporate quantitatively all the chitosan droplets. In contrast, the particles produced under the co-flow configuration exhibited only one size mode, suggesting that the chitosan and welding nanoparticles formed a single new structure. In Fig. 3, the chitosan droplets are shown to be nearly quantitatively incorporated with welding nanoparticles. This implies that nearly quantitative incorporation of the welding nanoparticles and chitosan droplets into a single structure may be possible at co-current flow in the presence of an orifice just after their mixing.

TEM images (Fig. 4) indicate that the model welding particles were agglomerates (consisting of primary metallic particles), whereas the chitosan particles were spherical, with a smooth surface. In the case of the “mixed A” particles, the welding particles

were redistributed in the chitosan matrix due to deagglomeration (by setting the force acting on an agglomerate of size  $D_{pa}$  due to the sudden pressure change across an orifice in the collision atomizer), and the size is given by [21]

$$D_{pr} = \alpha \sqrt{\frac{D_{pa}H}{6\pi\Delta P\Theta^2}} \quad (4)$$

where  $D_{pr}$  is the size of a restructured agglomerate,  $\alpha$  is the proportionality constant,  $H$  is the Hamaker constant,  $\Delta P$  is the pressure difference between the front and the rear of the orifice, and  $\theta$  is the parameter controlling the maximum cohesive strength between the constituting particles in an agglomerate. Agglomerated welding particles passed through the orifice, and the rapid changes in pressure, density, and velocity across the orifice produced an impulse

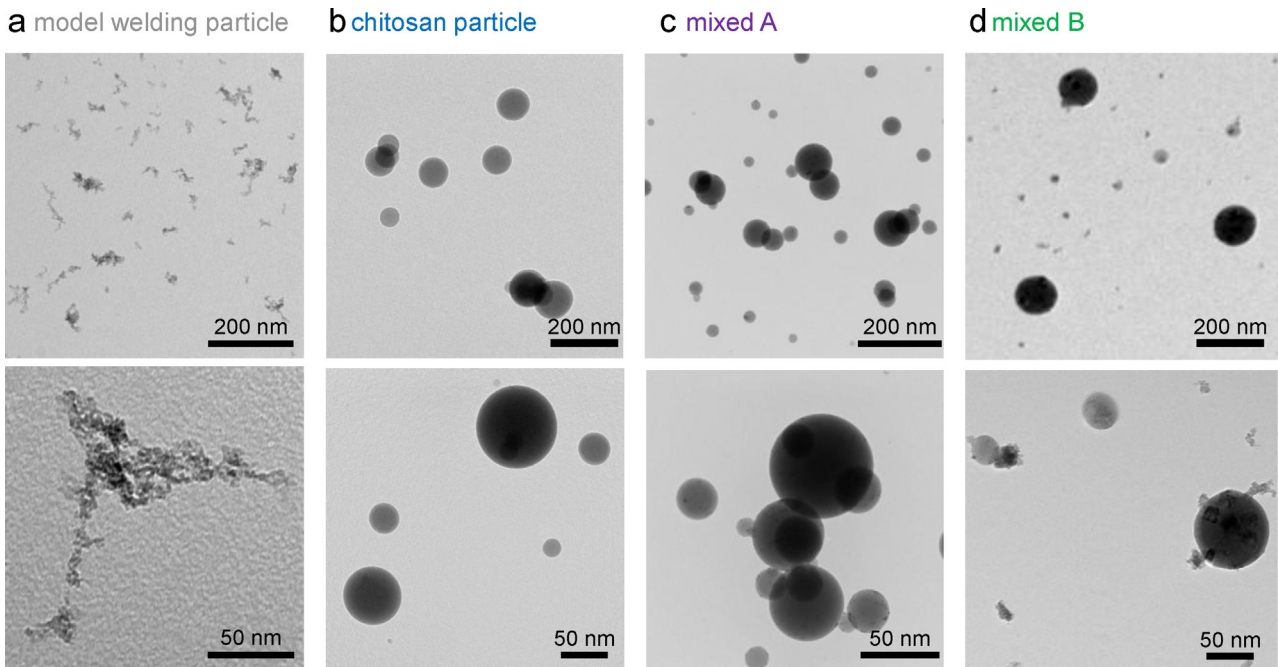


**Fig. 4.** Low and high magnification TEM images of spark produced model welding nanoparticles, collision atomized chitosan particles, and their mixing in a co-flow (mixing A) or counter-flow (mixing B) configuration.

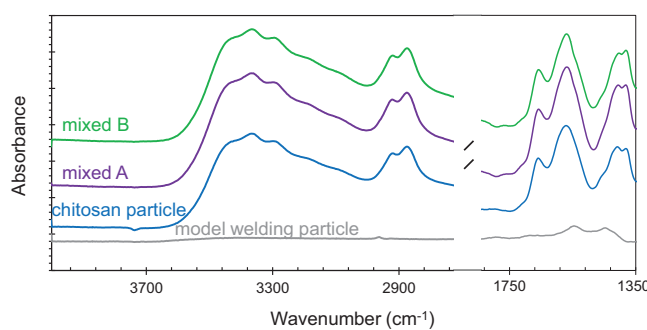


**Fig. 5.** FTIR spectra of spark produced model welding nanoparticles, collision atomized chitosan particles, and their mixing in a co-flow (mixing A) and counter-flow (mixing B) configuration.

capable of shattering the agglomerates. Size distributions like that shown in the high magnification TEM image of the “mixed A” case could be attained, if the particles were encapsulated with chitosan at the orifice and agglomeration was reduced [21]. In the case of “mixed B (counter-current flow),” unlike the “mixed A (co-current flow)” situation, heterogeneous agglomeration between the welding and chitosan components induced a simply collided structure (i.e. welding particles on a chitosan particle).

To investigate the chemical properties of mixed particles, measurements of IR spectra of pure welding and chitosan particles, and of the mixtures (Fig. 5). Welding particles show a featureless spectrum at the given absorbance scales, but weak bands around at 1400 cm<sup>-1</sup> probably correspond to iron oxide particles [22–24]. For individual chitosan particles, on the other hand, the IR spectrum clearly exhibits the typical absorption bands at 3360, 2920, and 2880 cm<sup>-1</sup>, which represent, respectively, the stretching vibrations of –OH, –CH<sub>2</sub>, and –CH<sub>3</sub> groups [25]. Characteristic bands at 1680, 1560, and 1380 cm<sup>-1</sup> can be assigned to amide I, amide

II, and amide III, respectively. The peaks at 1410 and 1310 cm<sup>-1</sup> correspond to the vibrations of the –OH and –CH groups in the pyranose ring. These characteristic peaks still remained after incorporation between the welding and chitosan components, implying a passivation of the welding particles with chitosan. The average cell viability after exposure to the individual welding and chitosan particles, and their mixtures, were evaluated using a fluorescence microscope for A549 cells at different concentrations, such as 5, 20, 50, 100, and 200 µg mL<sup>-1</sup> (Fig. 6). In all cases, average cell viability decreased as concentration increased for a given particle type. Average cell viability ranged from 96 ± 4.6% to 88 ± 5.3% for chitosan nanoparticles and 77 ± 8.1–42 ± 4.1% for model welding particles. Whereas, different average viabilities ranged from 96 ± 5.8% to 87 ± 6.2% for the “mixed A” particles and 87 ± 6.8–61 ± 3.9% for the “mixed B” particles have been observed.

In addition, there are no significant differences in cytotoxicity between the chitosan and the “mixed A” samples. Moreover, a better performance (co-flow reduced more than counter-flow) from the “mixed A” particles in toxicity reduction than that from “mixing B” particles may have originated from a degree of passivation. The “mixed B” particles are more cytotoxic than the “mixed A” and chitosan alone. This may be explained using TEM images shown in Fig. 4, as it is apparent, the welding particles may be attached to the surface of the chitosan particles and not fully incorporated as in “mixed A.” Incorporation between the welding and chitosan particles in the co-flow condition induced a better coverage of the chitosan on welding particles. The higher toxicity of the welding particles is considered to be a consequence of damage from the interaction with plasma membranes or other cellular compartments. Metallic (especially Fe, Mn, Cr, and Ni in this work, refer to Table 2) nanoparticles are known catalysts of oxidative stress in cells; oxidative species are generated which, interacting with metal, elicit redox-cycling cascades, and thus induce single-strand breaks in DNA [26–28]. From the results, a spray device of chitosan

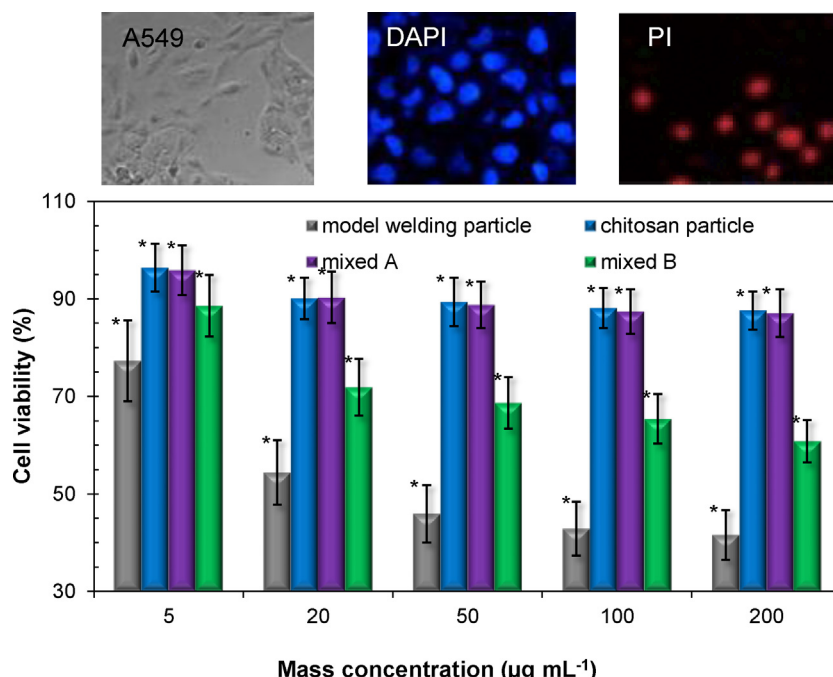


**Fig. 6.** Profiles in in vitro average cell viability from exposure to spark produced model welding nanoparticles, collision atomized chitosan particles, and their mixing in a co-flow (mixing A) counter-flow (mixing B) configuration in A549 cells. The figure also contains sample microscope images of A549 cells and their treated samples with DAPI and PI. Average cell viability tests were replicated twice with triplicate repeated measurements, and thus, the error bars derived from the repeated measurements. The *p* values of model welding particle, chitosan particle, mixed A, and mixed B are 0.0429, 0.0457, 0.0456, and 0.0468, respectively. The results are shown as mean ± SD and *p* < 0.05 was regarded as statistically significant compared to the untreated control. MTT absorbance of untreated control cells (cells incubated with CCM only) was set at 1 to determine relative number of viable cells.

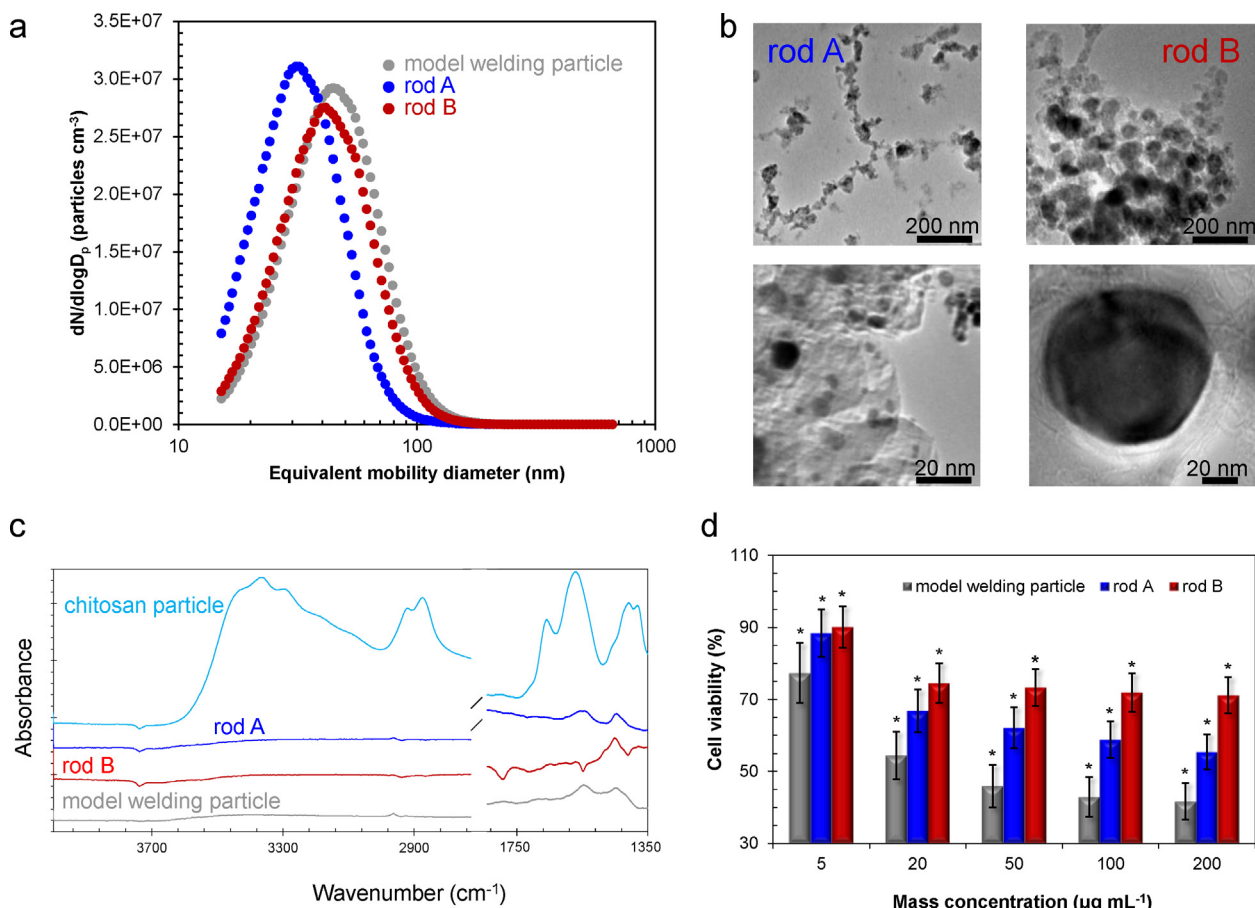


**Fig. 7.** Results of other passivations with the insertion of chitosan adhesive (rod A) or graphite paste (rod B) in a welding rod being used for spark discharge. (a) Size distributions. (b) Low and high magnification TEM images. (c) FTIR spectra. (d) Profiles in vitro average cell viability. The *p* values of rod A and rod B are 0.0496 and 0.0479, respectively. The results are shown as mean  $\pm$  SD and *p* < 0.05 was regarded as statistically significant compared to the untreated control. MTT absorbance of untreated control cells was set at 1 to determine relative number of viable cells.

**Table 2**  
Elemental compositions of model welding nanoparticles.

Element	Atomic ratio
Fe	0.44 $\pm$ 0.07
Mn	0.25 $\pm$ 0.06
Cr	0.22 $\pm$ 0.04
Ni	0.09 $\pm$ 0.04

Atomic ratio was determined using EDX mapping for nanoparticle sampled substrate. The results are shown as mean  $\pm$  SD.

solution to be installed on a welding protector or mask might be considerable for reducing health risks from welding nanoparticles.

Fig. 7a summarizes the size distributions of spark produced nanoparticles from the second type of passivation. The GMD, GSD, and TNC of the nanoparticles are summarized in Table 3. The

**Table 3**

A summary of the size distributions of spark produced model welding nanoparticles and other spark configurations using insertion of chitosan adhesive (rod A) or graphite paste (rod B) in a welding rod.

Case	GMD <sup>a</sup> (nm)	GSD <sup>b</sup>	TNC <sup>c</sup> (cm <sup>-3</sup> )
Model welding particle	43.9 $\pm$ 1.2	1.54 $\pm$ 0.02	1.40 $\times$ 10 <sup>7</sup>
Rod A	32.4 $\pm$ 0.8	1.48 $\pm$ 0.01	1.38 $\times$ 10 <sup>7</sup>
Rod B	41.0 $\pm$ 1.0	1.53 $\pm$ 0.01	1.31 $\times$ 10 <sup>7</sup>

<sup>a</sup> Results are expressed as mean  $\pm$  SD from at least three independent experiments.

<sup>a</sup> Geometric mean diameter.

<sup>b</sup> Geometric standard deviation.

<sup>c</sup> Total number concentration.

modification of the cathode generated a change in the size distribution. Both size distributions from the modifications shifted to smaller sizes compared to that of the individual welding particles, and the chitosan adhesive inserted case (rod A) showed a larger difference in size distribution than that in the case of rod B. This suggests that the sublimation of the chitosan or graphite component may induce a different mechanism of particle formation which may allow gas-phase incorporation of chitosan or graphite into the metallic particles. Low- and high-magnification TEM images are shown in Fig. 7b, which verifies the different formation of the particles. In the case of "rod A", spherical dark particles (metallic component) are seen as spots on another material, and the support material may have originated from the sublimation of chitosan adhesive, while the spherical dark particles are encapsulated by several graphitic layers in the case of "rod B". Details of the particle formation of graphitic carbon encapsulated metallic particles in the metal-graphite plasma process could be found in previous reports [15]. To verify the feasibility of the incorporation of chitosan (or graphite) component on a welding particle, measurements of the IR spectra of the "rod A" and "rod B" cases were also performed (Fig. 7c). Small peaks compared with chitosan particles at around 1550 (–CH<sub>2</sub>) and 1400 (C—OH) cm<sup>-1</sup> from "rod A" and peaks around at 1750 (C=C vibration) and 1400 (C—OH) cm<sup>-1</sup> from "rod B" may be attributed to the incorporation of chitosan adhesive and graphite paste on welding particles, respectively. The weakened characteristic peaks of chitosan for the "rod A" might have originated from graphitization of carbonaceous component of chitosan on welding particles. Unlike chitosan particles, graphite showed

a featureless spectrum at the given absorbance scales [29]. The average cell viability from exposure to nanoparticles from both the “rod A” and “rod B” samples was further evaluated to verify the effectiveness in toxicity reduction at the different concentrations (Fig. 7d). Results show that the range of average cell viability was  $88 \pm 5.9$ – $55 \pm 5.0\%$  and  $90 \pm 6.6$ – $71 \pm 5.1\%$  for nanoparticles from the “rod A” and “rod B” cases, respectively. In addition, the range of average cell viabilities from chitosan adhesive and graphite paste was  $94.4 \pm 3.9$ – $82.3 \pm 4.3\%$  and  $91.2 \pm 3.4$ – $75.9 \pm 5.5\%$ , respectively. This implies that the modification of the welding rod may also induce reduction of the nanoparticle toxicity in vitro. A better performance in toxicity reduction for the “rod B” case may have originated from a degree of passivation, similar to the incorporation of chitosan. As seen in TEM images shown in Fig. 7b, a nearly complete overlay with graphitic layers on welding particles may efficiently prevent the release of toxic components from the welding particles into cells. On this account, biocompatible component containing welding rods might be helpful to reduce health risks from the inhalable nanoparticles if their welding properties are remained to be acceptable.

#### 4. Conclusion

For the first time, the reduction in cytotoxicity of inhalable engineered nanoparticles via gas-phase in situ passivation of the nanoparticle surface with biocompatible materials was verified with in vitro measurements. The nanoparticle passivation with chitosan exhibited a lower toxicity in lung cancer cell line compared to the model welding nanoparticles alone by interfering the direct contact between the welding nanoparticles and cells. This work also demonstrates that the configuration in chitosan incorporation (e.g., co-current flow, counter-current flow, welding rod modification) may influence the ability of chitosan to modify toxicity. These results will provide some useful evidence for the efficient reduction of inhalable toxic components from engineered nanoparticles, which would be generalizable to a broad range of occupational health management for a variety of environments.

#### Acknowledgement

This work was partially supported by National Science Foundation (NSF) Grant CHE-0924431.

#### References

- [1] M.-H. Lee, W.J. McClellan, J. Candela, D. Andrews, P. Biswas, Reduction of nanoparticle exposure to welding aerosols by modification of the ventilation system in a workplace, *J. Nanopart. Res.* 9 (2007) 127–136.
- [2] D. Stephenson, G. Seshadri, J.M. Veranth, Workplace exposure to submicron particle mass and number concentrations from manual arc welding of carbon steel, *AIHA J.* 64 (2003) 516–521.
- [3] S.S. Leonard, B.T. Chen, S.G. Stone, D. Schwegler-Berry, A.J. Kenyon, D. Frazer, J.M. Antonini, Comparison of stainless and mild steel welding fumes in generation of reactive oxygen species, Part. Fibre Toxicol. 7 (2010) 32.
- [4] T. Wittczak, J. Walusiak, C. Palczynski, Welding-related respiratory diseases, *Med. Pr.* 60 (2009) 201–208.
- [5] M. Zhang, L. Jian, P. Bin, M. Xing, J. Lou, L. Cong, H. Zou, Workplace exposure to nanoparticles from gas metal arc welding process, *J. Nanopart. Res.* 15 (2013) 2016.
- [6] J.M. Antonini, J.R. Roberts, S. Stone, B.T. Chen, D. Schwegler-Berry, R. Chapman, P.C. Zeidler-Erdely, R.N. Andrews, D.G. Frazer, Persistence of deposited metals in the lungs after stainless steel and mild steel welding fume inhalation in rats, *Arch. Toxicol.* 85 (2011) 487–498.
- [7] K.-M. Yu, N. Topham, J. Wang, M. Kalivoda, Y. Tseng, C.-Y. Wu, W.-J. Lee, K. Cho, Decreasing biotoxicity of fume particles produced in welding process, *J. Hazard. Mater.* 185 (2011) 1587–1591.
- [8] M.D. Taylor, J.R. Roberts, S.S. Leonard, X. Shi, J.M. Antonini, Effects of welding fumes of differing composition and solubility on free radical production and acute lung injury and inflammation in rats, *Toxicol. Sci.* 75 (2003) 181–191.
- [9] J.F.P. Gomes, P.C.S. Albuquerque, R.M.M. Miranda, M.T.F. Vieira, Determination of airborne nanoparticles from welding operations, *J. Toxicol. Environ. Health Part A* 75 (2012) 747–755.
- [10] K.R. Carpenter, B.J. Monaghan, J. Norrish, Analysis of fume formation rate and fume particle composition for gas metal arc welding (GMAW) of plain carbon steel using different shielding gas compositions, *ISIJ Int.* 49 (2008) 416–420.
- [11] J.M. Antonini, A.A. Afshari, S. Stone, B. Chen, D. Schwegler-Berry, W.G. Fletcher, W.T. Goldsmith, K.H. Vandestouwe, W. McKinney, V. Castranova, D.G. Frazer, Design construction, and characterization of a novel robotic welding fume generator and inhalation exposure system for laboratory animals, *J. Occup. Environ. Hyg.* 3 (2006) 194–203.
- [12] A.K. Suresh, D.A. Pelletier, W. Wang, J.L. Morrell-Falvey, B. Gu, M.J. Doktycz, Cytotoxicity induced by engineered silver nanocrystallites is dependent on surface coatings and cell types, *Langmuir* 28 (2012) 2727–2735.
- [13] R. Jayakumar, D. Menon, K. Manzoor, S.V. Nair, H. Tamura, Biomedical applications of chitin and chitosan based nanomaterials – a short review, *Carbohydr. Polym.* 82 (2010) 227–232.
- [14] A. Grenha, C.I. Grainger, L.A. Dailey, B. Seijo, G.P. Martin, C. Remuñán-López, B. Forbes, Chitosan nanoparticles are compatible with respiratory epithelial cells in vitro, *Eur. J. Pharm. Sci.* 31 (2007) 73–84.
- [15] J.H. Byeon, J.H. Park, K.Y. Yoon, J. Hwang, Ambient spark generation to synthesize carbon encapsulated metal nanoparticles in continuous aerosol manner, *Nanoscale* 1 (2009) 339–343.
- [16] J.H. Park, I.A. Mudunkotuwa, J.S. Kim, A. Stanam, P.S. Thorne, V.H. Grassian, T.M. Peters, Physicochemical characterization of simulated welding fumes from a spark discharge system, *Aerosol Sci. Technol.* 48 (2014) 768–776.
- [17] S. Tashiro, T. Zeniya, K. Yamamoto, M. Tanaka, K. Nakata, A.B. Murphy, E. Yamamoto, K. Yamazaki, K. Suzuki, Numerical analysis of fume formation mechanism in arc welding, *J. Phys. D: Appl. Phys.* 43 (2010) 434012.
- [18] S.C. Tan, E. Khor, T.K. Tan, S.M. Wong, The degree of deacetylation of chitosan: advocating the first derivative UV-spectrophotometry method of determination, *Talanta* 45 (1998) 713–719.
- [19] J.H. Byeon, J.T. Roberts, Aerosol based fabrication of biocompatible organic–inorganic nanocomposites, *ACS Appl. Mater. Interfaces* 4 (2012) 2693–2698.
- [20] A. Lauto, J. Hook, M. Doran, F. Camacho, L.A. Poole-Warren, A. Avolio, L.J.R. Foster, Chitosan adhesive for laser tissue repair: in vitro characterization, *Lasers Surg. Med.* 36 (2005) 193–201.
- [21] J.H. Byeon, J.T. Roberts, Aerosol based fabrication of thiol-capped gold nanoparticles and their application for gene transfection, *Chem. Mater.* 24 (2012) 3544–3549.
- [22] S. Kayal, R.V. Ramanujan, Anti-cancer drug loaded iron–gold core–shell nanoparticles (Fe@Au) for magnetic drug targeting, *J. Nanosci. Nanotechnol.* 10 (2010) 5527–5539.
- [23] A.L. Willis, N.J. Turro, S. O’Brien, Spectroscopic characterization of the surface of iron oxide nanocrystals, *Chem. Mater.* 17 (2005) 5970–5975.
- [24] S.J. Parikh, J. Chorover, ATR-FTIR spectroscopy reveals bond formation during bacterial adhesion to iron oxide, *Langmuir* 22 (2006) 8492–9500.
- [25] A.P.P. Praxedes, R.C. da Silva, R.P.A. Lima, J. Tonholo, A.S. Ribeiro, I.N. de Oliveira, Effects of UV irradiation on the wettability of chitosan films containing dansyl derivatives, *J. Colloid Interface Sci.* 376 (2012) 255–261.
- [26] A.L. Guildford, T. Poletti, L.H. Osbourne, A.D. Cerbo, A.M. Gatti, M. Santin, Nanoparticles of a different source induce different patterns of activation in key biochemical and cellular components of the host response, *J. R. Soc. Interface* 6 (2009) 1213–1221.
- [27] M. Pumera, Nanotoxicology: the molecular science point of view, *Chem. Asian J.* 6 (2011) 340–348.
- [28] B. Berlinger, N. Benker, S. Weinbruch, B. L'Vov, M. Ebert, W. Koch, D.G. Ellingsen, Y. Thomassen, Physicochemical characterisation of different welding aerosols, *Anal. Bioanal. Chem.* 399 (2011) 1773–1780.
- [29] J.H. Byeon, J.-W. Kim, Ambient plasma synthesis of  $\text{TiO}_2$ @graphite oxide nanocomposites for efficient photocatalytic hydrogenation, *J. Mater. Chem. A* 2 (2014) 6939–6944.